Processing Map and Performance of a Low-Cost Wrought Magnesium Alloy: ZAXEM11100

Thomas Avey, Jiashi Miao, Joshua Caris, Anil K. Sachdev, and Alan Luo

Abstract

Lightweight components improve the fuel efficiency of internal combustion vehicles and contribute to extending the driving range of electrified vehicles. Many Mg alloys have been developed over the years to meet these demands; however, low formability at room temperature, corrosion, and high cost have inhibited widespread adoption in the automotive industry. The new alloy Mg-1Zn-1Al-0.5Ca-0.2Ce-0.4Mn (ZAXEM 11100, all in weight %) has shown excellent post-rolling formability with an Ericksen Index of 7.8 mm and a post-T6 yield stress of 270 MPa in lab scale sheet samples. In this work, a processing map based on Gleeble thermomechanical tests has been developed for the new alloy. This processing map provided important guidance to a production scale extrusion. This work details the mechanical performance of ZAXEM11100 as an extrusion alloy.

Keywords

Extrusion • Magnesium alloys • Processing map

T. Avey · J. Miao · A. Luo (✉)
Department of Materials Science and Engineering, The Ohio State University, Columbus, OH 43210, USA
e-mail: luo.445@osu.edu

J. Caris
Terves LLC, Euclid, OH 44117, USA

A. K. Sachdev
General Motors Global Research and Development, Warren, MI 48092, USA

A. Luo
Department of Integrated Systems Engineering, The Ohio State University, Columbus, OH 43210, USA

Introduction

Vehicle lightweighting has been a strong motivator for magnesium alloy development as a lightweight material [1, 2]. With increasing demand and production of electric vehicles, where large capacity and heavy batteries are needed, the benefit of removing weight from other areas of the vehicle has become a greater initiative [3]. Magnesium (Mg) and its alloys have been formed successfully into automotive parts by both high-pressure die casting (HPDC) and wrought processing [1, 4]. A major hurdle toward greater use of Mg has been its low formability at room temperature, largely due to strong c-axis texture after deformation [4, 5]. This has limited the use of wrought Mg to only higher temperature production methods like rolling, forging, and extrusion [6]. The increase in working temperature can improve formability but will also increase processing time, cost, and complexity compared to steel and aluminum alloys. [1]

Currently, there are very few commercial wrought Mg alloy compositions, compared to steel and Al alloys, used for structural applications [4, 5, 7]. The most common are the Al- and Zn-containing alloys (AZ61, AZ80, AZ31), Zn- and Zr-containing alloys (ZK60, ZK31), and Al- and Mn-containing alloys (AM30). Extensive research has been conducted into modifications to these alloys with rare earths, Li, and/or Ca [8–12]. These additions have shown improvement in room temperature ductility and formability [4, 12]. This is due to the ability of these elements to modify texture of the deformed microstructure, the CRSS of slip systems, and the occurrence and frequency of twinning.

Shi et al. [5], in cooperation with the United States Automotive Materials Partnership (USAMP), developed Mg-1Zn-1Al-0.5Ca-0.4Mn-0.2Ce alloy (all in weight %, hereafter referred to as ZAXEM11100) that possessed high formability in post-rolled T4 condition and excellent tensile properties after T6. The improved formability was credited to texture modifications (Ca and Ce in solid solution) and the

S. Barela et al. (eds.), *Magnesium Technology 2023*, The Minerals, Metals & Materials Series,
https://doi.org/10.1007/978-3-031-22645-8_35

improved strength post-heat treatment to clustering of solute atoms.

Forming at elevated temperatures makes possible deformation modes that are not readily activated at room temperature. In wrought Mg-Zn-Al alloys, deformed at elevated temperatures, Dynamic Recovery (DRV), Dynamic Recrystallization (DRX), and Dynamic Precipitation (DP) have been reported each with different and interdependent effects on flow behavior [13, 14]. The processing map was developed to display the dominate microstructure mechanisms that are acting at a given process conditions (temperature and strain rate) [15–17].

The current paper extends the work on this alloy begun by Shi et al. by observing the compressive stress vs. strain behavior under various temperatures and strain rates to produce a processing map. The extrudability and scalability of this alloy is studied with large-scale extrusion testing.

Numerical Methods

Processing Map Construction

A processing map is a well-studied tool for hot working processes, which can be used to find the optimal temperature and strain rates for deformation [18]. The maps are constructed with two parts: an efficiency parameter and a stability criterion [19–21]. Most published processing maps make use of the Prasad method [22] due in part to the computational simplicity as well as the large body of literature to support its reliability. A brief derivation of the important equations is given as well as a discussion as to important assumptions made in the derivation that must be satisfied. The assumptions of the processing maps are that the work piece acts as a power dissipator, where the total applied power (P) is dissipated by plastic work/heat and microstructural change, through irreversible processes. This process is expressed as:

$$P = \sigma \cdot \dot{\varepsilon} = \int_0^{\dot{\varepsilon}} \sigma * d\dot{\varepsilon} + \int_0^{\sigma} \dot{\varepsilon} * d\sigma \tag{1}$$

which can also be written more simply as

$$P = G + J \tag{2}$$

with G being the dissipator content and represents the power dissipated by plastic work (heat) and J being the dissipator co-content which represents the power dissipated by dynamic microstructural and metallurgical processes. J is the term of interest and can be evaluated as

$$J = \int_0^{\sigma} \dot{\varepsilon} * d\sigma = \frac{\sigma * \dot{\varepsilon} * m}{m+1} \tag{3}$$

under the assumption of a power-law stress–strain rate relationship ($\sigma = A\dot{\varepsilon}^m$). The simplification in Eq. 3 is only valid if strain rate ($\dot{\varepsilon}$) and the strain rate sensitivity parameter (m) are independent. This independence can be verified by plotting $\ln(\sigma)$ versus $\ln(\dot{\varepsilon})$. If $\dot{\varepsilon}$ and m are independent, the resulting curve will be linear and the efficiency that power is dissipated by microstructural processes, η, is defined by Prasad as the ratio

$$\eta = \frac{J}{J_{\max}} = \frac{2m}{m+1} \tag{4}$$

where $J_{\max}$ is the value of J at $m = 1$ or where the workpiece acts as a liner dissipator. However, if $\dot{\varepsilon}$ and m are not independent, both Eqs. 3 and 4 are invalid. To compute processing maps in this case, Murty and Rao et al. developed a more general solution that does not rely on the power-law relationship [23]. Equation 4 was modified to be

$$\eta = \frac{J}{J_{\max}} = \frac{(P-G)}{J_{\max}} = 2\left[1 - \frac{1}{\sigma * \dot{\varepsilon}} \int_0^{\dot{\varepsilon}} \sigma d\dot{\varepsilon}\right] \tag{5}$$

Equation 5 requires an integration of G beginning at a strain rate of zero which is not done experimentally. To mediate this, Murty and Rao separated the integral in Eq. 5 so that a power-law relationship is assumed near a strain rate of zero via Eq. 6 and substituted into Eq. 5.

$$G_o = \frac{1}{m+1}\sigma\dot{\varepsilon} \tag{6}$$

$$\begin{aligned} \eta &= 2\left[1 - \frac{1}{\sigma * \dot{\varepsilon}} \int_0^{\dot{\varepsilon}} \sigma d\dot{\varepsilon}\right] \\ &= 2\left[1 - \frac{1}{\sigma * \dot{\varepsilon}} \left(\int_0^{\dot{\varepsilon}_{\min}} \sigma d\dot{\varepsilon} + \int_{\dot{\varepsilon}_{\min}}^{\dot{\varepsilon}} \sigma d\dot{\varepsilon}\right)\right] \\ &= 2\left[1 - \frac{1}{\sigma * \dot{\varepsilon}} \left(G_0 + \int_{\dot{\varepsilon}_{\min}}^{\dot{\varepsilon}} \sigma d\dot{\varepsilon}\right)\right] \end{aligned} \tag{7}$$

There are many proposed equations to predict instability for the construction of processing maps [24]. Kumar [19] and Prasad [20] built on the instability criteria outlined by Ziegler [25]

$$\frac{dD}{d\dot{\varepsilon}} > \frac{D}{\dot{\varepsilon}} \tag{8}$$

where $D(\dot{\varepsilon})$ is the materials dissipative function which is substituted for J as the metallurgical dissipative function is

of interest. The full derivation can be found in the cited literature. This substitution in a power-law stress and strain rate relationship yields the inequality

$$\xi(\dot{\varepsilon}) = \frac{d\ln\left(\frac{m}{m+1}\right)}{d\ln\dot{\varepsilon}} + m > 0 \quad (9)$$

wherever this inequality is not satisfied, instable flow is predicted to occur. When the power law relationship is not assumed, the stability criteria is seen in Eq. 10 as derived by Murty and Rao [24].

$$2m > \eta \quad (10)$$

Materials and Methodology

The material used for this study was gravity cast ZAXEM11100 alloy billets (22.86 cm diameter by 76.2 cm length) provided by Terves LLC. The composition was verified with spark optical emission spectroscopy (Spark-OES) and is included in Table 1. A test billet was subjected to a multistage heat treatment, developed in a previous work [5], to sequentially dissolve all secondary phases and improve processability.

Compression cylindrical samples were machined by electronic discharge machining (EDM) to the size of 10 mm diameter by 15 mm long. Samples were taken near the outer edge of the heat-treated billet slice. Uniaxial compression tests at fixed temperatures and true strain rates were performed on a Gleeble 3800 thermomechanical testing frame. The test temperatures were from 325 to 425 °C in 25 °C increments and strain rates in one-decade increments from 10^{-3} to 10^{0} s^{-1}. Strain was measured by using the displacement of the Gleeble arm. All compression tests were conducted to a true strain of 1 mm/mm. Samples were resistively heated at a rate of 5 °C/s until the desired temperature was reached. The temperature was measured with a thermocouple that was impact welded to the center of the sample. All sample temperatures remained within ±3 °C throughout testing. After testing, samples were quenched into room temperature water within 5 s of test termination to prevent post-deformation microstructure evolution.

Large-scale extrusions were done on an Extral 3800 MT extrusion press. The billets were skinned with a lathe to remove scaling before preheating to 390 °C. A 0.4″ × 5.5″ (1 × 13.9 cm) plate die with at extrusion ratio of 28.9 was used. Feed rate was varied to change the average strain rate, as calculated through slab analysis, of the extrusion from 0.04 to 0.15 s^{-1}.

Results and Discussion

Figure 1 shows the flow behavior of ZAXEM11100 alloy, following an expected trend of yield stress and flow stress decreasing with increasing temperature and increasing with increasing strain rate. The flow stress data was first processed with a custom-built MATLAB program using a cubic spline fit to extrapolate the experimental data to intermediate strain rates and temperatures. After this extrapolation, a $\ln(\sigma)$ versus $\ln(\dot{\varepsilon})$ plot, Fig. 2, was constructed, and ZAXEM11100 was determined to not follow a linear relationship, and, therefore, the Murty and Rao method for processing map construction (Eq. 7) and the instability relationship from Eq. 10 will be used in this work.

The flow stress data at 20, 40, 60, and 80% strains was used to construct the processing maps seen in Fig. 3. Two domains and one instability region were identified by conventional means. Domain I has a maximum efficiency 0.95–1, exists at low strain rate (10^{-3} s^{-1}), and shifts from 350 to 375 °C as the strain increases. The peak efficacy of Domain II cannot be determined because the bulk of this domain is at strain rates higher than the tested rates. The bulk of the processing map is dominated by the instability region. This region exists between strain rates of $10^{-2.7}$ s^{-1} to 10^{-1} s^{-1} at all temperatures investigated with little movement seen in location the instability region at different strains.

Generally, curves at low strain rates (10^{-3}–10^{-2}) and high temperatures (400–425 °C) show ideal plastic flow behavior while curves at 10^{0} strain rate and 325–375 °C show strain softening that is evidence of dynamic microstructural changes. The early peak in flow stress followed by softening seen in 10^{-2} s^{-1}, 325 °C condition and the 10^{0} s^{-1}, 425 °C both show strong evidence for significant DDRX [26] (Fig. 1).

The power of a processing map is its ability to identify regions ideal for extensive deformation processing. Conventional wisdom is to select strain rates and temperatures that result in a high degree of DRX. In Mg alloys, this is even more important due to the reduced *c*-axis texture and grain size of heavily recrystallized microstructures. A peak efficiency between 30 and 50%, depending on the material's stacking fault energy, is a good indication for DRX being the dominating microstructural process [22]. Domain II could be an option as the efficacy seen in the range investigated is in the 30–50% range that is typical of good dynamic recrystallization [18].

Table 1 OES measured composition of ZAXEM11100 billet

Element	Zn	Al	Ca	Ce	Mn	Other elements	Mg
Composition (wt.%)	1.38	1.25	0.52	0.2	0.46	0.09	96.1

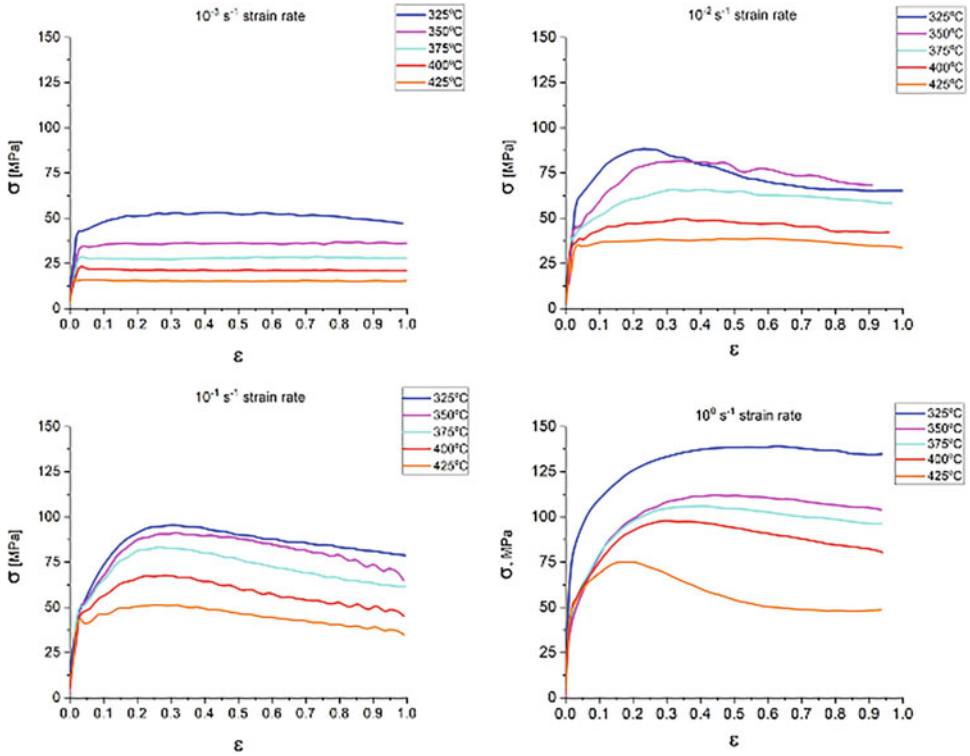

Fig. 1 True stress vs strain plots of ZAXEM 11100 at strain rates of **a** 10^{-3} s^{-1}, **b** 10^{-2} s^{-1}, **c** 10^{-1} s^{-1}, and **d** 10^{0} s^{-1}

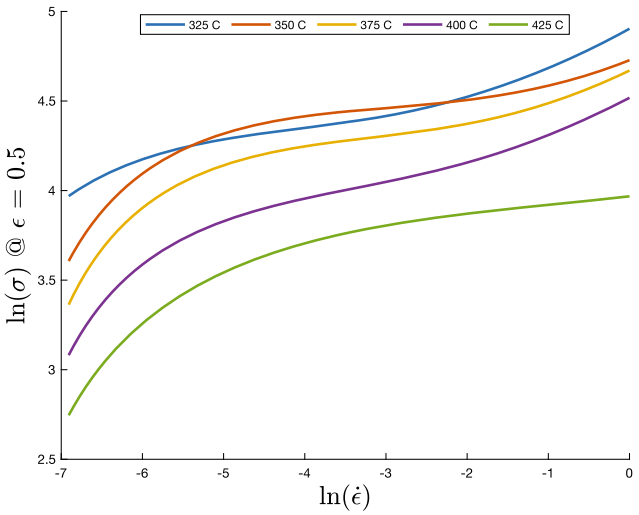

Fig. 2 $\ln(\sigma)$ versus $\ln(\dot{\epsilon})$ plot of ZAXEM11100 at a fixed true strain of 0.5

Production Scale Extrusions

A pilot study of the performance of this alloy under industrial scale extrusion was performed on the same billet with the same condition used in the production of the processing map. The first trial was done with a billet temperature of 390 °C and a speed of 1″/min (25.4 mm/min). There was no observed macroscopic cracking, Fig. 4a. A second trial was done at the same billet temperature but with an elevated extrusion speed of 2″/min (50.8 mm/min). This second trial, Fig. 4b, resulted in extensive hot cracking after extrusion despite the calculated average strain rate, 0.15 s^{-1}, and extrusion temperature falling within the stable region of the processing map except for the initial strains, Fig. 3a.

Through CALPHAD analysis Fig. 5, the solidus of ZAXEM11100 was calculated to be quite low at 425 °C. The measured temperature of the plate, after leaving the extrusion press, fluctuated between 420 and 450 °C which is 60 °C warmer than the billet before extrusion and above the solidus temperature indicating that friction during extrusion resulted in sufficient heating induce incipient melting. A lower initial billet temperature was attempted but the stress required to begin extrusion, breakthrough stress, was too great and extrusion was not possible. In Table 2, the effect of Zn and Ca content on the solidus was investigated. It was found that reduction of each individually was able to raise the solidus to above the exit temperature of the billet at 2″/min.

While ZAXEM11100 has shown good performance in lab scale rolling experiments and some promise in the processing map analysis, the low solidus gives it a very narrow temperature range for successful production scale extrusion. A change in the Zn or Ca content could increase this window and lead to a more extrudable alloy.

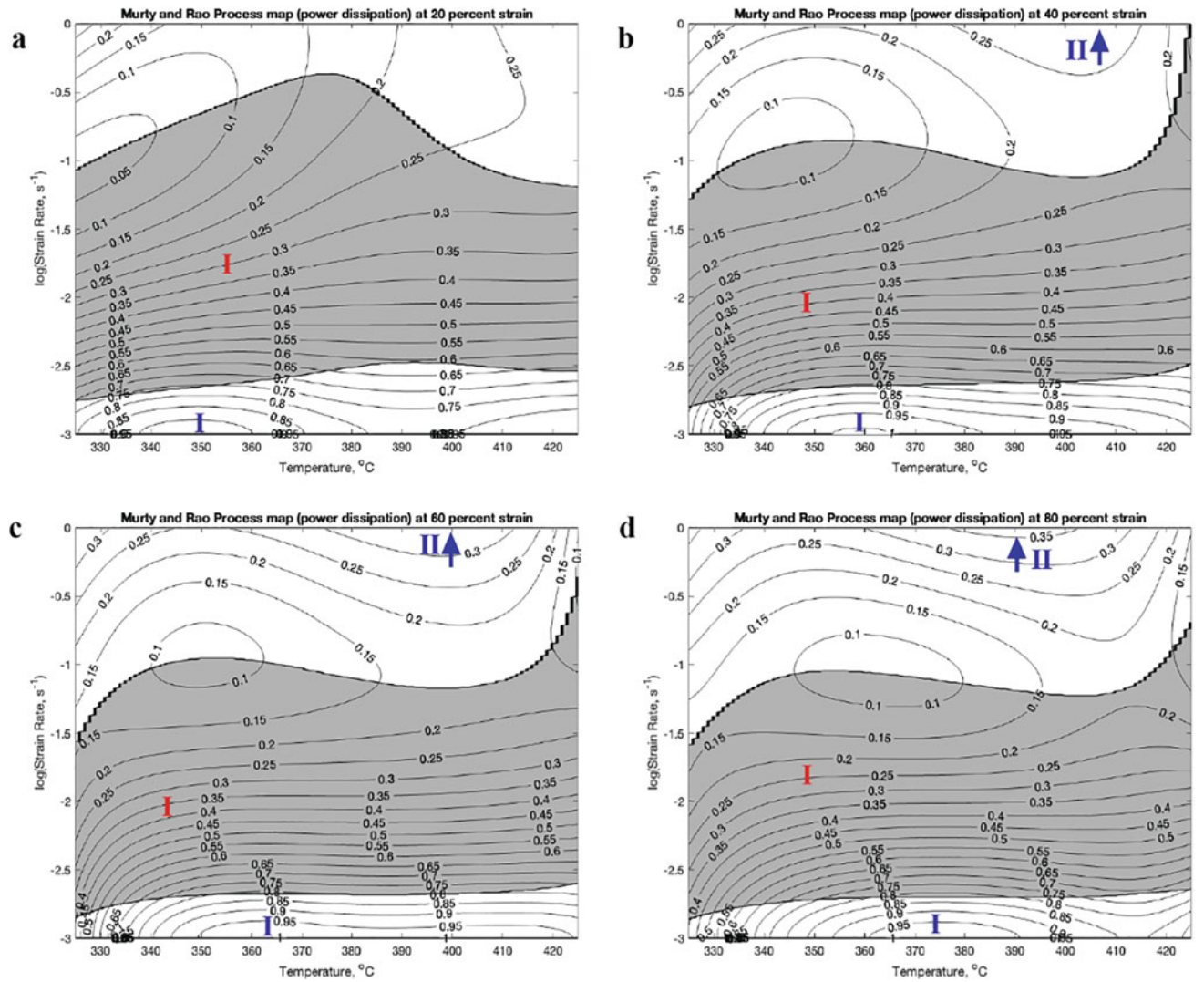

Fig. 3 Processing map Constructed for ZAXEM11100 at **a** 20%, **b** 40%, **c** 60%, and **d** 80% strain with the instability region shaded in gray. Contour lines correspond to lines of equal efficiency

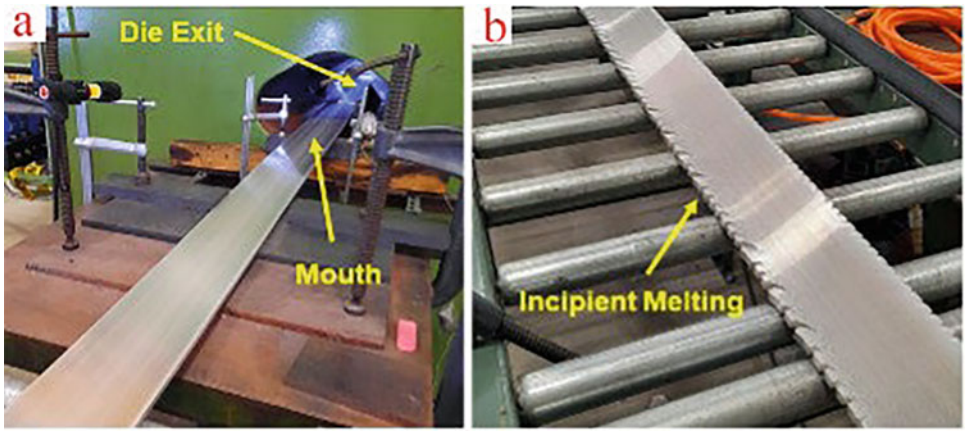

Fig. 4 Images of extruded ZAXEM11100 plate as it left the die with an extrusion speed of **a** 1``/min (25.4 mm/min) and **b** 2'/min (50.8 mm/min)

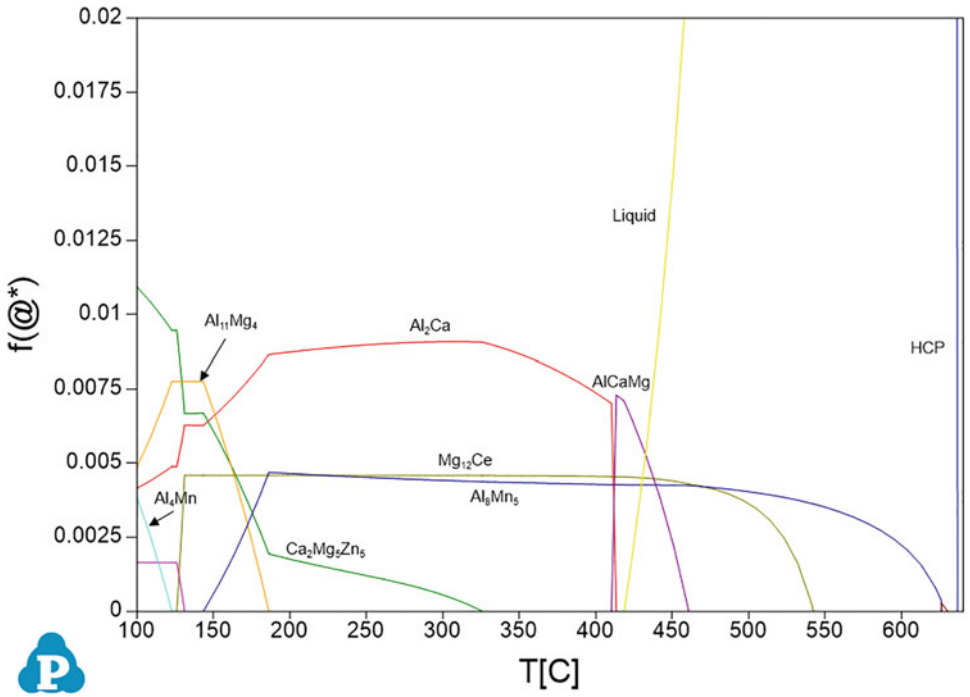

Fig. 5 Equilibrium phase fraction versus temperature plot of ZAXEM11100 billet used in extrusion testing calculated with the PanMg2021 database

Table 2 Effect of Zn and Ca content on the solidus of nominal ZAXEM11100 composition (Mg-1Zn-1Al-0.5Ca-0.2Ce-0.4Mn)

Zn content (wt%)	Solidus temp (°C)	Ca content (wt%)	Solidus temp (°C)
0.7	465	0	570
1	442	0.5	442
1.4	417		

Conclusions

An investigation of the processing feasibility of ZAXEM11100 was conducted through lab scale thermo-mechanical testing and through production scale extrusions.

- ZAXEM11100 does not exhibit a linear strain sensitivity parameter and therefore needs to be modeled with the less conventional but more general solution developed by Murty and Rao [23].
- The resulting processing map shows a wide instability region from 350 to 425 °C and at strain rates between $10^{-2.5}$ and 10^{-1} s^{-1}.
- Production scale extrusion found that extrusion speed was limited by incipient melting resulting from frictional heating and ZAXEM11100's low solidus temperature.
- CALPHAD analysis was done, and the solidus of ZAXEM11100 was shown to be very sensitive to Zn and Ca content.
- The thermal window to successfully extrude ZAXEM11100 limits its usability but a change to the Zn or Ca composition should improve its workability.

Acknowledgements Funding for this work was provided by DOE project award DE-SC0020806. This report was prepared as an account of work sponsored by an agency of the United States government. Neither the United States government nor any agency thereof, nor any of their employees, makes any warranty, express or implied, or assumes any legal liability or responsibility for the accuracy, completeness, or usefulness of any information, apparatus, product, or process disclosed, or represents that its use would not infringe privately owned rights. Reference herein to any specific commercial product, process, or service by trade name, trademark, manufacturer, or otherwise does not necessarily constitute or imply its endorsement, recommendation, or favoring by the United States government or any agency thereof. The views and opinions of authors expressed herein do not necessarily state or reflect those of the United States government or any agency thereof.

References

1. Joost WJ, Krajewski PE. Towards magnesium alloys for high-volume automotive applications. Scr Mater 2017;128:107–12. https://doi.org/10.1016/J.SCRIPTAMAT.2016.07.035.
2. Taub A, De Moor E, Luo A, Matlock DK, Speer JG, Vaidya U. Materials for Automotive Lightweighting. Annu Rev Mater Res 2019;49:327–59. https://doi.org/10.1146/annurev-matsci-070218-010134.
3. Muratori M, Alexander M, Arent D, Bazilian M, Cazzola P, Dede EM, et al. The rise of electric vehicles—2020 status and future expectations. Prog Energy 2021;3:022002. https://doi.org/10.1088/2516-1083/ABE0AD.

4. Luo AA, Shi R, Miao J, Avey T. Review: Magnesium Sheet Alloy Development for Room Temperature Forming. JOM 2021;73:1403–18. https://doi.org/10.1007/s11837-021-04616-y.
5. Shi R, Miao J, Avey T, Luo AA. A new magnesium sheet alloy with high tensile properties and room-temperature formability. Sci Rep 2020;10:1–10. https://doi.org/10.1038/s41598-020-67161-9.
6. Pekguleryuz MO. Current developments in wrought magnesium alloys. Woodhead Publishing Limited; 2012. https://doi.org/10.1533/9780857093844.1.3.
7. Luo AA. Applications: Aerospace, automotive and other structural applications of magnesium. Fundam. Magnes. Alloy Metall. A Vol. Woodhead Publ. Ser. Met. Surf. Eng., Elsevier Inc.; 2013, p. 266–316. https://doi.org/10.1533/9780857097293.266.
8. Bettles CJ, Gibson MA. Current wrought magnesium alloys: Strengths and weaknesses. JOM 2005 575 2005;57:46–9. https://doi.org/10.1007/S11837-005-0095-0.
9. Liu C, Chen X, Chen J, Atrens A, Pan F. The effects of Ca and Mn on the microstructure, texture and mechanical properties of Mg-4 Zn alloy. J Magnes Alloy 2021;9:1084–97. https://doi.org/10.1016/J.JMA.2020.03.012.
10. Meng X, Wu R, Zhang M, Wu L, Cui C. Microstructures and properties of superlight Mg–Li–Al–Zn wrought alloys. J Alloys Compd 2009;486:722–5. https://doi.org/10.1016/J.JALLCOM.2009.07.047.
11. Liu P, Jiang H, Cai Z, Kang Q, Zhang Y. The effect of Y, Ce and Gd on texture, recrystallization and mechanical property of Mg–Zn alloys. J Magnes Alloy 2016;4:188–96. https://doi.org/10.1016/J.JMA.2016.07.001.
12. Mishra RK, Gupta AK, Rao PR, Sachdev AK, Kumar AM, Luo AA. Influence of cerium on the texture and ductility of magnesium extrusions. Scr Mater 2008;59:562–5. https://doi.org/10.1016/J.SCRIPTAMAT.2008.05.019.
13. He YY, Fang G. Characterization of dynamic precipitation behaviors accompanying dynamic recrystallization in an Mg-Al-Zn-RE alloy. J Alloys Compd 2022;901:163745. https://doi.org/10.1016/j.jallcom.2022.163745.
14. Myshlyaev MM, Mcqueen HJ, Mwembela A, Konopleva E. Twinning, dynamic recovery and recrystallization in hot worked MgÁ/ AlÁ/ Zn alloy. Mater Sci Eng A 2002;337:121–33.
15. Ashby MF. A first report on deformation-mechanism maps. Acta Metall 1972;20:887–97. https://doi.org/10.1016/0001-6160(72)90082-X.
16. Fatemi SM, Aliyari S, Miresmaeili SM. Dynamic precipitation and dynamic recrystallization during hot deformation of a solutionized WE43 magnesium alloy. Mater Sci Eng A 2019;762:138076. https://doi.org/10.1016/J.MSEA.2019.138076.
17. Mohamed FA, Langdon TG. Deformation mechanism maps based on grain size. Metall Mater Trans B 1974 511 1974;5:2339–45. https://doi.org/10.1007/BF02644014.
18. Sutton SC, Luo AA. Constitutive behavior and processing maps of a new wrought magnesium alloy ZE20 (Mg-2Zn-0.2Ce). J Magnes Alloy 2020;8:111–26. https://doi.org/10.1016/j.jma.2019.11.007.
19. Kumar AKSK. Criteria for Predicting Metallurgical Instabilities in Processing. Master's Thesis. India Institute of Science, Bangalore, India, 1987.
20. Prasad YVRK, Gegel HL, Doraivelu SM, Malas JC, Morgan JT, Lark KA, et al. Modeling of Dynamic Material Behavior in Hot Deformation: Forging of Ti-6242. n.d.
21. Prasad YVRK. Recent Advances in the Science of Mechanical processing. Indian J Technol 1990;28:435–51.
22. Prasad Y, Rao K, Sasidhar S. Hot working guide: a compendium of processing maps. ASM international; 2015.
23. Murty SVSN, Sarma MS, Rao BN. On the evaluation of efficiency parameters in processing maps. Metall Mater Trans A Phys Metall Mater Sci 1997;28 A:1581–2. https://doi.org/10.1007/s11661-997-0219-y.
24. Narayana Murty SVS, Nageswara Rao B, Kashyap BP. Instability criteria for hot deformation of materials. Int Mater Rev 2000;45:15–26. https://doi.org/10.1179/095066000771048782.
25. Zeigler H. Progress in solid mechanics. New York: Wiley; 1963.
26. Huang K, Logé RE. A review of dynamic recrystallization phenomena in metallic materials. Mater Des 2016;111:548–74. https://doi.org/10.1016/j.matdes.2016.09.012.